2023 62nd IEEE Conference on Decision and Control (CDC)
December 13-15, 2023. Marina Bay Sands, Singapore

Tutorial on dynamics and control of grid-connected power electronics and renewable generation

Dominic Groß

Abstract— **Electrical power systems are transitioning from fuel-based generation to renewable generation and transmission interfaced by power electronics. This transition challenges standard power system modeling, analysis, and control paradigms across timescales from milliseconds to seasons. This tutorial focuses on frequency stability on timescales of milliseconds to seconds. We first review basic results for grid-following (GFL) and grid-forming (GFM) control of voltage source converters (VSCs), typical renewable generation, and high voltage direct current (HVdc) transmission. In this context, it becomes apparent that GFL and GFM control functions are needed to operate emerging power systems. However, combining GFL resources, GFM resources, and legacy generation on the same system results in highly complex dynamics that are a significant obstacle to stability analysis. The remainder of the tutorial provides an overview of recent developments in universal GFM controls that bridge the gap between GFL and GFM control and provide a pathway to a coherent control and analysis framework accounting for power generation, power conversion, and power transmission.**

I. INTRODUCTION

The rapid integration of renewable generation and power electronics into electric power systems challenges standard system models, controls, analysis methods, and operating paradigms [1]–[4]. A much-discussed barrier to a sustainable power system is the intermittency and variability of renewable generation, such as wind and solar. The resulting challenges on time scales of seconds to seasons are generally expected to be addressed through a mix of energy storage [2], demand side management [5], and leveraging geographic diversity of generation and load [6]. However, unlike past evolutions of power systems, the transition to converter-interfaced renewables replaces the very foundation of electric power systems (i.e., synchronous machines) with technologies with significantly different properties (i.e., power electronics). This unprecedented transition results in significantly different dynamics on time scales of milliseconds to seconds and jeopardizes system stability and reliability [1], [3], [4].

The existing literature has largely framed the resulting challenges from the viewpoint of (i) control of individual power converters when abstracting power generation and power systems as ideal voltage sources [7], (ii) power system dynamics [1], [8] and system-level stability analysis [4], [9], [10] when abstracting power conversion and (renewable) generation as controlled voltage or current sources, and (iii) control of renewable generation when abstracting power converters as controlled current sources feeding power into a power system that is not explicitly modeled [11]–[13]. Although these perspectives have proven useful for developing controls for power electronics and renewable generation, they do not provide a complete view of the interactions of heterogeneous power generation (e.g., steam turbines, solar PV, wind turbines), power conversion (e.g., machines, power electronics), and power transmission (e.g., ac and HVdc).

Today, most renewables are interfaced by dc/ac voltage source converters (VSC) using so-called grid-following (GFL) control to control their power injection and stabilize the power source of the converter at an operating point that maximizes renewable energy generation or minimizes HVdc losses. This class of controls assumes a slowly changing grid frequency and voltage irrespective of the power injection by renewables and, ultimately, jeopardizes grid stability [3]. In contrast, so-called grid-forming (GFM) VSCs impose ac voltage dynamics at their grid terminal that self-synchronize through the power network and are envisioned to be the cornerstone of future power systems [3], [4]. However, loosely speaking, standard GFM controls require a fully controllable dc power source and may destabilize the system due to power source dynamics or limits [14], [15].

From this viewpoint, standard GFL and GFM controls provide complementary functions that are needed to operate power systems that contain a mix of converter-interfaced renewable generation and transmission as well as conventional generation. However, the resulting system dynamics can be highly complex and interoperability of converter-interfaced resources and system stability are a major concern. Moreover, analytical methods typically only consider networks of GFM VSCs with ideal power sources, or individual GFL VSCs interfacing renewable generation to an idealized grid. Thus far, only numerical works considered (i) the interactions between various power conversion technologies and their controls through the power system [8], [16], [17], or (ii) the interaction of renewable generation with limited controllability, power converter controls, and aggregate power system frequency dynamics [15], [18], [19]. These works highlight the need for control design and end-to-end analysis methods that account for the key salient features and interactions of power generation, power conversion, and their interaction through power transmission. This tutorial provides (i) an introduction to modeling of solar PV, wind power, and HVdc from a control point of view, (ii) applications of GFL and GFM control, and (iii) an introduction to recent work on universal GFM control that unifies key functions of GFL and GFM control for renewable generation [20], [21] and HVdc [21]–[23], and enables an end-to-end frequency stability

This material is based upon work supported by the National Science Foundation under Grant No. 2143188.

D. Groß is with the Department of Electrical and Computer Engineering, University of Wisconsin-Madison, USA dominic.gross@wisc.edu

analysis using reduced-order models [21], [24].

II. Device and System Models

To clarify the role of different technologies, we first review standard models for renewable and legacy generation, machines and power electronics, as well as ac and dc transmission.

A. Legacy and renewable power generation

Legacy bulk power generation is based on different turbine technologies (e.g., steam, hydro) and speed governors that are commonly represented using the reduced-order model

$$T_{\mathrm{m}} \tfrac{\mathrm{d}}{\mathrm{d}t} P_{\mathrm{m}} = -P_{\mathrm{m}} + P_{\mathrm{m}}^{\star} K_{\mathrm{m}} (\omega - \omega_0), \tag{1}$$

with mechanical power $P_{\mathrm{m}} \in \mathbb{R}$, power setpoint $P_{\mathrm{m}}^{\star} \in \mathbb{R}$, turbine time constant $T_{\mathrm{m}} \in \mathbb{R}$, and speed governor gain $K_{\mathrm{m}} \in \mathbb{R}_{>0}$, turbine speed $\omega \in \mathbb{R}$, and nominal speed $\omega_0 \in \mathbb{R}$. While (1) is commonly used for system-level stability analysis, it neglects turbine dynamics that result in additional low pass filtering and, in the case of hydro turbines, non-minimum phase dynamics [25, Ch. 9].

The mechanical power $P_{\mathrm{wt}} \in \mathbb{R}$ generated by the wind turbine (WT) blades is typically modeled by [11]

$$P_{\mathrm{wt}} = C_p(\lambda, \beta) \tfrac{1}{2} \rho \pi R^2 v_{\mathrm{w}}^3, \tag{2}$$

with blade pitch angle $\beta \in \mathbb{R}$, density of air $\rho \in R_{>0}$, rotor radius $R \in R_{>0}$, and wind speed v_{w}. Moreover, using the WT rotor speed ω, we define the so-called tip speed ratio $\lambda = R\omega / v_{\mathrm{w}}$ and function $C_p : \mathbb{R}_{>0} \times \mathbb{R}_{>0} \to \mathbb{R}_{>0}$ that models the mechanical power on the WT rotor as a fraction of the available wind power [11]. Strictly speaking, (2) is only valid in steady-state. Dynamics arising from dynamic inflow may be captured by including lead-lag filters [26]. The pitch angle β is controlled by a motor with control input $u_\beta \in \mathbb{R}$ typically modeled as a lowpass filter [11].

Finally, the current generated by photovoltaics is given by

$$i_{\mathrm{pv}} = i_{\mathrm{L}} - i_0 \big(\exp(\tfrac{v_{\mathrm{dc}} + R_s i_{\mathrm{pv}}}{\alpha v_t}) - 1 \big) - \tfrac{v_{\mathrm{dc}} + R_s i_{\mathrm{pv}}}{R_p}, \tag{3}$$

where $v_{\mathrm{dc}} \in \mathbb{R}_{\geq 0}$ denotes the dc voltage applied to the PV panel and $i_{\mathrm{L}} \in \mathbb{R}_{\geq 0}$ denotes the photogenerated current. Here $i_0 \in \mathbb{R}_{\geq 0}$, $v_t \in \mathbb{R}_{>0}$, $R_s \in \mathbb{R}_{>0}$, $R_p \in \mathbb{R}_{>0}$, and $\alpha \in \mathbb{R}_{>0}$ denote the saturation current, thermal voltage, series and parallel resistances, and diode ideality factor [27]. The nonlinear characteristics of PV and a WT are shown in Fig. 1.

B. Electromechanical power conversion

For conventional generation (1), synchronous machines are used to convert mechanical power to electrical. Synchronous machines induce a (balanced) three-phase ac voltage $v_{\mathrm{m}} \in \mathbb{R}^3$ behind the machine stator impedance (see Fig. 2a) with phase angle $\angle v_{\mathrm{m}} = \theta_{\mathrm{m}}$ and magnitude $V_{\mathrm{m}} \in \mathbb{R}_{\geq 0}$ (controlled through an excitation system). The machine speed $\tfrac{\mathrm{d}}{\mathrm{d}t} \theta_{\mathrm{m}} = \omega_{\mathrm{m}} \in \mathbb{R}$ is commonly modeled by the swing equation

$$J_{\mathrm{m}} \omega_0 \tfrac{\mathrm{d}}{\mathrm{d}t} \omega_{\mathrm{m}} = -D_{\mathrm{m}} \omega_{\mathrm{m}} + P_{\mathrm{m}} - P_{\mathrm{ac}} \tag{4}$$

with inertia constant $J_{\mathrm{m}} \in \mathbb{R}_{>0}$, damping constant $D_{\mathrm{m}} \in \mathbb{R}$ that models windage losses, and active (electric) power $P_{\mathrm{ac}} \in \mathbb{R}$ flowing into the grid. While this reduced-order linearized model is useful for analyzing and understanding frequency dynamics, its validity has always been a subject of debate. Please see [28], [29], [4, Sec. 2.2.1] for a detailed discussion of machine models and further references.

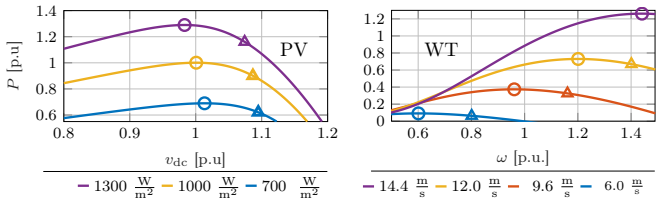

Fig. 1: Power generation of PV (left) as a function of dc voltage and irradiation (i.e., i_{L}) and a wind turbine (right) as a function of rotor speed and wind speed (zero blade pitch). Circles and triangles indicate the maximum power point (MPP) and typical operating points with 10% curtailment.

C. AC/DC power conversion

While the controls in this tutorial apply to more complex topologies (see [22]), we focus on two-level VSCs. Two-level VSCs are controlled by a modulation signal $m \in \{-1, 1\}^3$ actuating on/off states of semiconductor switches [30, Ch. 5] that modulate a dc voltage v_{dc} into a three-phase voltage $v_{\mathrm{sw}} = m v_{\mathrm{dc}}$. The resulting switching ripple is commonly suppressed by an inductive-capacitive output filter (see Fig. 2b). The dynamics of the VSC dc-link voltage with dc-link capacitance $c_{\mathrm{dc}} \in \mathbb{R}_{>0}$ are modeled by

$$c_{\mathrm{dc}} v_{\mathrm{dc}}^{\star} \tfrac{\mathrm{d}}{\mathrm{d}t} v_{\mathrm{dc}} = P_{\mathrm{dc}} - P_{\mathrm{ac}}. \tag{5}$$

In practice, modulation techniques (e.g., pulse width modulation) are used to compute the discrete switching signal m at high switching frequencies[1] to, on average, approximate a continuous reference for v_{sw}. Assuming a high enough switching frequency relative to the remaining system dynamics, the converter voltage $v_{\mathrm{sw}} \in \mathbb{R}^3$ is typically averaged over one switching period to obtain an averaged model that is tractable for control design and analysis [30, Ch. 2.5].

[1]Typically ranging from 1 kHz for high power/medium voltage two-level VSCs to 10 kHz for low power/voltage two-level VSCs.

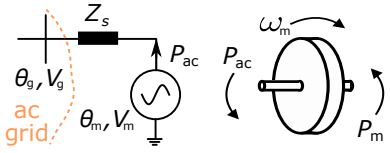

(a) synchronous machine

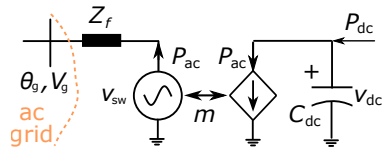

(b) voltage source converter

Fig. 2: System-level models of a synchronous machine (a) and a two-level voltage source converter (b).

Controls that have been designed using averaged models can often be directly applied by, e.g., using notch and lowpass filters to remove the remaining ripple at the switching frequency from voltage and current measurements. However, care needs to be taken when investigating phenomena on fast time scales (e.g., response to electrical faults) for VSCs with low switching frequency. Moreover, VSCs are typically controlled using inner control loops (see Fig. 3) to either (i) track a voltage reference with phase angle θ and magnitude $V \leq \frac{1}{2} v_{\text{dc}}$ on their filter terminal, or (ii) control the power injection P_{ac} [7].

D. Controllability and inherent energy storage

Overall, it can be seen that both synchronous machines and voltage source converters convert power between different domains. Synchronous machines typically store significant kinetic energy $\frac{1}{2} J \omega_{\text{m}}^2$ (i.e., in the range of 2 s to 12 s times rated power) but can only be actuated at low bandwidth through (i) the mechanical power $P_{\text{m}} \in \mathbb{R}$, and (ii) the excitation system that controls the voltage magnitude $V_{\text{m}} \in \mathbb{R}$. In contrast, the energy $\frac{1}{2} c_{\text{dc}} v_{\text{dc}}^2$ stored in the dc-link capacitor of VSCs is relatively small (i.e., in the range of 5 ms to 70 ms times rated power) but the VSC ac voltage can be fully actuated with high bandwidth through the control input m.

E. Network topology and power exchange

It remains to model the ac and dc power exchange through ac and dc networks as a function of the ac and dc voltages applied by the power conversion devices (i.e., synchronous machines and VSCs). Arguably, the most accurate model represents the network as distributed parameter system [31]. However, this model is generally seen as intractable for simulation and analysis beyond highly stylized systems. Thus, for stability analysis, the power network is typically modeled by an undirected graph $\mathcal{G} = (\mathcal{N}, \mathcal{E})$ with node set $\mathcal{N}$ representing buses (i.e., locations at which devices and/or circuit branches interconnect) of the power system and edge set $\mathcal{N} \subseteq \mathcal{E} \times \mathcal{E}$ representing circuit branches (i.e., machine stator, converter output filter, transmission line, cables, and transformers). In this framework, a potential (i.e., voltage) is associated with every node $l \in \mathcal{N}$ and a flow (i.e., current or power) is associated with every edge $(l, k) \in \mathcal{E}$. Models of various fidelity can be associated with the nodes and edges. For example, fitted frequency domain

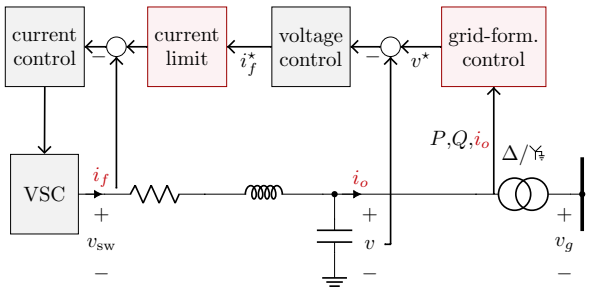

Fig. 3: Cascaded inner VSC control that tracks a voltage reference provided by an outer GFM control.

models that accurately capture the dynamics of ac and dc transmission for frequencies up to 1 MHz are commonly used when detailed simulations are required [32], [33]. In contrast, commonly used first-principles models often account for network circuit dynamics by modeling branches and buses through ordinary differential equation models of inductors and capacitors or generating units [34], [35]. The vast majority of the literature neglects the circuit dynamics and models the network through power flow models that model the steady state of the underlying network circuit dynamics. This model is commonly justified by the pronounced timescale separation between synchronous generators and circuit dynamics [4], [36]. Moreover, for analysis of high-voltage ac systems power flow models are further simplified by neglecting transmission losses. This results in the lossless ac power flow model

$$P_{\text{ac},l} = \sum\nolimits_{(k,l)\in\mathcal{E}_{\text{ac}}} V_l V_k b_{k,l} \sin(\theta_l - \theta_k) + P_{d,\text{ac},l}, \qquad (6)$$

where $b_{k,l} \in \mathbb{R}_{\geq 0}$ denotes the susceptance of the ac line $(k,l) \in \mathcal{E}_{\text{ac}} \subseteq \mathcal{E}$, $\mathcal{E}_{\text{ac}} \in \mathcal{N}_{\text{ac}} \times \mathcal{N}_{\text{ac}}$ denotes the set of ac lines, and $P_{d,\text{ac}} \in \mathbb{R}$ models load. Moreover, with a slight abuse of notation relative to the device models, we use θ_l and V_l to denote the voltage phase angle and magnitude at bus $l \in \mathcal{N}_{\text{ac}}$, where $\mathcal{N}_{\text{ac}} \subseteq \mathcal{N}$ denotes the set of ac buses. Similarly, using $\mathcal{N}_{\text{dc}}$ to denote dc buses, $v_{\text{dc},l}$ to denote the voltage of dc bus $l \in \mathcal{N}_{\text{dc}}$, and $g_{k,l} \in \mathbb{R}_{\geq 0}$ to denote the conductance of a dc line $k, l \in \mathcal{E}_{\text{dc}} \subseteq \mathcal{E}$ with $\mathcal{E}_{\text{dc}} \in \mathcal{N}_{\text{dc}} \times \mathcal{N}_{\text{dc}}$, results in [37]

$$P_{\text{dc},l} = v_{\text{dc},l} \sum\nolimits_{(k,l)\in\mathcal{E}_{\text{dc}}} g_{k,l}(v_{\text{dc},l} - v_{\text{dc},k}). \qquad (7)$$

We emphasize that (6) and (7) neglect losses and the circuit dynamics of the network. While this assumption is commonly made in control design and stability analysis of grid-connected power electronics, this model cannot capture instabilities that arise from interactions of the network circuit dynamics with VSC controls [38]–[41]. Neglecting the network circuit dynamics is typically justified for high voltage and power levels [41]. In contrast, at lower power and voltage levels the network circuit dynamics cannot be neglected unless a sufficient timescale separation between the network and VSCs is enforced through controls [38], [40]. Similarly, losses are typically negligible for high-voltage systems but significantly impact dynamics at lower voltage levels.

Finally, we note that (6) is commonly used to model balanced three-phase systems. Extensions to unbalanced multiphase systems for power flow studies can be found in [42], [43]. Moreover, a steady-state power network model that is tractable for analytical stability studies of systems containing three-phase and single-phase generating units and common three-phase transformer interconnections is described in [44].

F. Plant and power system models

The models developed in this section are the building blocks of an overall power system model that accounts for generation, conversion, and transmission (see Fig. 4) that can be combined by extending graph-based models to account for power conversion nodes (e.g., ac/dc VSCs) that convert between domains [21], [24]. Specifically, a multi-machine power system model is obtained by combining the

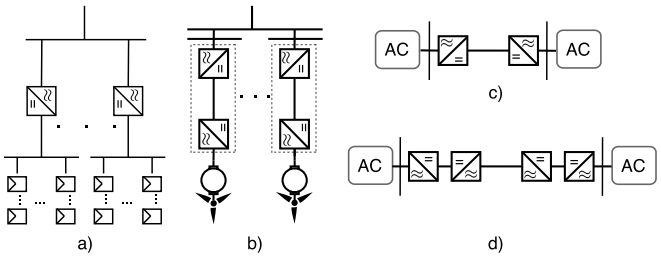

Fig. 4: a) PV plant and dc/ac VSCs b) wind farm with PMSG wind turbines c) HVdc transmission, and d) low frequency ac transmission [45].

turbine/governor model (1) with the synchronous machine model (4) and interconnecting the machines through the ac power flow equations (6). To model a single-stage PV system, the PV model (3) is combined with a VSC by letting $P_{\text{dc}} = v_{\text{dc}} i_{\text{pv}}$. Permanent magnet synchronous generator (PMSG) wind turbines can be modeled as an interconnection of two VSCs through (7) and a synchronous machine. Likewise, a point-to-point HVdc link can be modeled as an interconnection of two dc terminals of VSCs through (7).

III. Control objectives and paradigms

A. Control objectives

The control objectives for grid-connected power converters and renewables can be broadly categorized as follows.

Objective 1 (Maximizing energy yield) *Stabilize the power converter and its power source at an operating point that maximizes energy yield.*

For example, so-called maximum power point tracking (MPPT) aims to operate renewables at their MPP (see Fig. 1). In the context of HVdc, this objective corresponds to operating at maximum dc voltage to minimize losses.

Objective 2 (Grid support) *Stabilize the power converter and its power source at an operating point provided by a higher-level controller and contribute to stabilizing the system by autonomously responding to power imbalances.*

This objective applies to ac networks (e.g., primary frequency control) and HVdc networks (e.g., primary dc voltage control) and generally requires curtailment of renewable sources or energy storage to respond to power imbalances.

B. GFL and GFM control paradigm

Controls for grid-connected power electronics are broadly categorized into grid-following (GFL) and grid-forming (GFM) control. However, no universally agreed-upon definition of GFM and GFL exists. Early attempts at a definition require a GFM VSC to impose an ac voltage with constant amplitude and frequency [7]. Other definitions hinge on the ability to operate ac grids without relying on synchronous generators [3], the ability to suppress frequency oscillations [46], or high-level functional requirements [47]. However, GFM capabilities may also be defined in terms of forming a dc grid [37]. Attempting to resolve the conceptual differences between these definitions is outside the scope of this tutorial. Instead, we broadly categorize converter controls as follows.

Definition 1 (GFM and GFL control [22]) *For each VSC terminal (i.e., ac and dc), we refer to a VSC as GFM if it imposes a stable voltage at the terminal (i.e., ac-GFM or dc-GFM), and GFL if it has to rely on another device to stabilize the voltage at the terminal (i.e., ac-GFL or dc-GFL).*

While Objective 1 is often conflated with GFL and Objective 2 is often conflated with GFM control, Definition 1 highlights that GFM does not necessarily imply a full suite of grid-support functions but only requires imposing (marginally) stable ac or dc voltages.

IV. GFM and GFL control of converter-interfaced renewables and transmission

A. ac-GFL/dc-GFL control

Various ac-GFL/dc-GFL controls have been proposed in the literature that (i) transfer a prescribed amount of power between the VSC terminals [17], or (ii) provide grid-support functions similar to those provided by synchronous generators today [48]. This broad class of controls cannot meet either Objective 1 or 2 and will not be discussed further here.

B. ac-GFL/dc-GFM control

Today grid-connected renewables typically use ac-GFL/dc-GFM control designed under the assumption that the power system can be abstracted as an ac voltage with slowly varying frequency and magnitude whose sensitivity to the VSC power injection is negligible (see Fig. 5). Typically, a synchronous reference frame (SRF) phase-locked loop (PLL)[2] is used to obtain an estimate $\theta_{\text{PLL}} \in \mathbb{S}$ of the grid voltage phase angle $\theta_{\text{g}} \in \mathbb{S}$ (see Fig. 2b) and implement a proportional-integral (PI) current control in a rotating coordinate frame with angle $\theta_{\text{PLL}} \in \mathbb{S}$ [7, Fig. 3]. The ac current is then controlled to stabilize the VSCs dc voltage (5) and power source at the MPP or a curtailed operating point (see Fig. 6). This approach can be combined with suitable curtailment strategies or energy storage to provide typical ancillary services (e.g., primary frequency control) [11]–[13], [19]. However, if (i) the impedance between ac-GFL VSCs and SGs or ac-GFM VSCs increases (i.e., weak coupling), or (ii) the rating of ac-GFL VSC relative to SGs and ac-GFM VSCs increases, then the sensitivity of $\theta_{\text{g}} \in \mathbb{S}$ to the ac-GFL VSCs power injection $P_{\text{ac}} \in \mathbb{R}$ is no longer negligible and the system eventually becomes unstable [50]–[52].

C. AC-GFM/dc-GFL control

To address the challenges of ac-GFL control, ac-GFM controls the VSC as a self-synchronizing ac voltage source (see Fig. 7). Notably, near the nominal steady-state and for realistic tuning common ac-GFM controls (e.g., virtual synchronous machines [53] and dispatchable virtual oscillator

[2]We emphasize that the presence of a PLL is not indicative of ac-GFL control. For example, the ac-GFM virtual synchronous machine control proposed in [49] uses an auxiliary PLL.

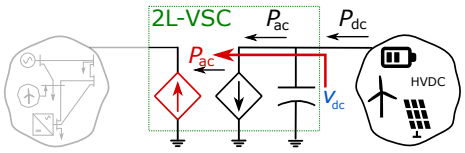

Fig. 5: Conceptually, ac-GFL/dc-GFM control assumes that the ac system is stable and stabilize the VSC power source.

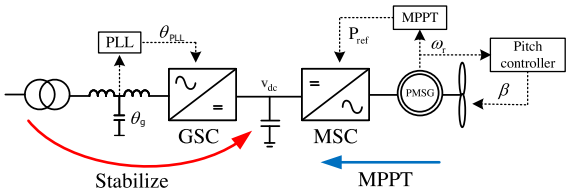

Fig. 6: PMSG wind turbine with ac-GFL/dc-GFM control on the grid-side converter (GSC) and MPPT control on the machine-side converter (MSC).

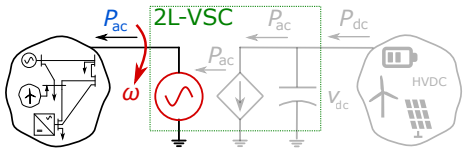

Fig. 7: Conceptually, ac-GFM/dc-GFL controls assumes that the VSC dc terminal is stable and stabilize the ac system.

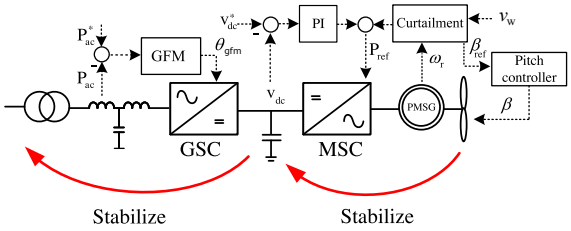

Fig. 8: PMSG wind turbine with ac-GFM/dc-GFL control on the grid-side converter (GSC) and dc voltage control on the machine side converter (MSC).

control [39]) resemble droop control [4, Sec. 3.4]

$$\frac{\mathrm{d}}{\mathrm{d}t}\theta_{\text{gfm}} = \omega_{\text{gfm}} = \omega_0 + m_p(P^\star_{\text{ac}} - P_{\text{ac}}). \tag{8}$$

Here, $\theta_{\text{gfm}} \in \mathbb{S}$ denotes a voltage phase angle reference, $m_p \in \mathbb{R}_{>0}$ is the active power droop coefficient, and $P^\star_{\text{ac}} \in \mathbb{R}$ denotes an active power setpoint provided by system-level controls. Notably, the reference $\theta_{\text{gfm}} \in \mathbb{S}$ is either directly modulated by the VSC (i.e., $\angle v_{\text{sw}} = \theta_{\text{gfm}}$) [54]–[56] or $\theta_{\text{gfm}} \in \mathbb{S}$ is used as a reference for the grid side filter voltage (i.e., v in Fig. 3) that is tracked by cascaded voltage and current PI controls [7], [53], [57]. Cascaded inner loops are often used to (i) ensure that the filter capacitor dynamics are well controlled, and (ii) leverage the inner current loop for current limiting [7]. While these features are appealing, stability of the cascaded control architecture intricately depends on the grid coupling strength [57]–[59]. Moreover, the required timescale separation between the various controls and dynamics [57] results in a significant loss of control bandwidth [58], [60].

Droop control (8) achieves voltage phase angle synchronization between ac-GFM converters through feedback of the power injection $P_{\text{ac}} \in \mathbb{R}$ (i.e., a function of phase angle differences) to its frequency ω_{gfm}. Moreover, (8) is identical to the turbine/governor system (1) with $T_{\text{m}} = 0$ and $K_{\text{m}} = 1/m_p$ and, e.g., results in an increased power injection $P_{\text{ac}} \in \mathbb{R}$ for a decrease in frequency $\omega_{\text{gfm}} \in \mathbb{R}$. To realize this response, (8) requires a controllable dc power source and may destabilize the system due to power source dynamics or limits [14]. To meet Objective 2 using renewable generation, various auxiliary power limiting and curtailment schemes have been developed that (i) limit the ac power $P_{\text{ac}} \in \mathbb{R}$ to the MPP of renewable sources [15], [18] and (ii) explicitly [15] or implicitly [18] control the VSC dc voltage through renewable sources (see Fig. 8). As of now, these approaches are tailored to specific renewables and generally require significant energy storage or curtailment, i.e., cannot meet Objective 1. Moreover, while ac-GFL is prone to instability under weak grid coupling, strong coupling (i.e., low impedance) between ac-GFM VSCs may result in instability due to interactions between network circuit dynamics and ac-GFM controls [38], [39], [57]. This instability can be avoided by increasing VSC output filter impedance, control re-tuning to increase the timescale separation between network circuit dynamics and ac-GFM control [41], [57], or active compensation of network circuit dynamics through control [41].

D. Interoperability of GFL and GFM control

In the literature, ac-GFM/dc-GFL and ac-GFL/dc-GFM control are commonly understood as complementary paradigms that are both required to operate a future power system with (i) renewable sources providing functions ranging from MPPT (ac-GFL/dc-GFM) to reliable grid-support (ac-GFM/dc-GFL), and (ii) converter-interfaced transmission such as HVdc that requires forming both ac and dc networks (see Fig. 9 and [37]). However, recent results highlighted a

Fig. 9: Standard HVdc control architecture.

wide range of potential instability mechanisms between ac-GFM/dc-GFL VSCs, ac-GFL/dc-GFM VSCs, SGs and their control loops, and ac network circuit dynamics [8], [16] even when neglecting dc-side and renewable generation dynamics. Similarly, systems using a mix of ac-GFM/dc-GFL and ac-GFL/dc-GFM VSCs to interconnect ac transmission systems through HVdc can become unstable due to changes in load or generation [17]. Overall, these results highlight that interoperability of ac-GFM/dc-GFL VSCs, ac-GFL/dc-GFM VSCs, renewable generation, HVdc, and SGs is not well understood from an applied and theoretical perspective.

V. Dual-port GFM control

Broadly speaking common ac-GFM controls aim to control VSCs to tightly control the frequency ω by mimicking

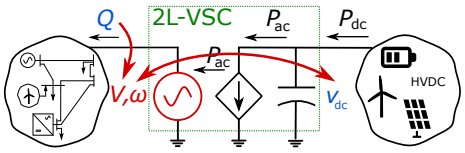

Fig. 10: Dual-port GFM control maps signals indicating power imbalance (i.e., ω and $v_{\rm dc}$) between the converter ac and dc terminals.

the active power response of the turbine/governor system (1) of conventional *power generation*. However, because the VSC is a *power conversion* device that cannot generate power, this results in instability if the VSC power source cannot supply the required power instantaneously [14]. Instead, recognizing the role of the VSC as a power conversion element, dual-port GFM control aims to controls the VSC ac and dc terminal voltages to ensure power balancing between the ac and dc terminal and induce a stabilizing response from curtailed renewable and legacy power generation.

A. Universal dual-port GFM control

In this tutorial, we focus on the dual-port GFM control

$$\omega_{\rm gfm} = \tfrac{\rm d}{{\rm d}t}\theta_{\rm gfm} = \omega_0 + k_\theta \tfrac{\rm d}{{\rm d}t} v_{\rm dc} + k_\omega (v_{\rm dc} - v_{\rm dc}^\star), \quad (9)$$

that maps the signals indicating power imbalances in ac and dc networks (i.e., $\omega_{\rm gfm}$ and $v_{\rm dc}$) between the VSC terminals (see Fig. 10). This control is equivalent to the PI control

$$\tfrac{\rm d}{{\rm d}t}\vartheta_{\rm dc} = v_{\rm dc} - v_{\rm dc}^\star, \quad \theta_{\rm gfm} = k_\theta (v_{\rm dc} - v_{\rm dc}^\star) + k_\omega \vartheta_{\rm dc} \quad (10)$$

from dc voltage to ac phase angle and, considering the lossless VSC model (5) and $P_{\rm ac}^\star = P_{\rm dc}$, it is identical to the control $\omega_{\rm gfm} = \omega_0 + k_\theta (P_{\rm ac}^\star - P_{\rm ac}) + k_\omega (v_{\rm dc} - v_{\rm dc}^\star)$ analyzed in [24]. Please see [21], [22] for a detailed comparison.

Similar controls were first proposed in the context of machine emulation control [55] that match the dynamics of a VSC to that of a synchronous machine by noting that the energy stored in the VSC dc-link capacitor, although being much smaller, plays the same role as the kinetic energy stored in the synchronous machine rotor (cf. (4) and (5)).

However, this mechanism has far wider-ranging implications. For example, using (9) on all VSCs in a network, an increase in load $P_{\rm ac} \in \mathbb{R}$ results in a decrease in dc voltage $v_{\rm dc}$ (see (5)) and ac frequency $\omega_{\rm gfm} \in \mathbb{R}$ that will propagate through ac and dc connections [21]–[23] to power generation as shown in Fig. 11. Thus, at a typical curtailed operating point as shown in Fig. 4, a PV system will increase its power generation in response to a drop in dc voltage [24]. Similarly, a wind turbine that is curtailed by operating at an increased rotor speed will increase its power production in response to a decrease in frequency [20], [21]. In contrast, for renewable generation operating at the MPP, the power generation will not respond and (9) will control the VSC dc voltage by implicitly controlling the ac power injection through the ac voltage phase angle $\theta_{\rm gfm} \in \mathbb{S}$ [20]. Overall, the key principle behind the control (9) is to propagate signals that indicate power imbalance throughout the power system and across power conversion elements until they eventually

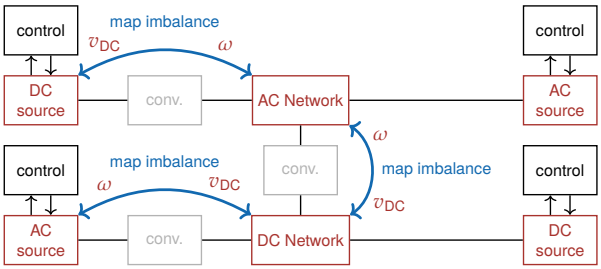

Fig. 11: Mapping of power imbalance signals between an ac network, dc network, and ac and dc power sources.

reach legacy or renewable power generation that responds to power imbalances by adjusting its power generation. This approach relies on the internal energy storage of VSCs and WTs as an energy buffer [21], [22] and investigating the impact of VSC and WT sizing is seen as an interesting topic for future work. Notably, as illustrated next, the control (9) also makes the dependence of the level of grid support provided by renewable generation on its operating point transparent.

B. Example: PMSG wind turbine

Applying dual-port GFM control to both the GSC and MSC of a PMSG wind turbine results in the control shown in Fig. 12. If the nominal frequency in (9) and pitch angle reference correspond to the MPP, this control results in approximate maximum power point tracking. In contrast, at a curtailed operating point (see Fig. 1) the wind turbine will provide primary frequency control. Moreover, below the wind turbine's rated wind speed, the rotor speed can be increased beyond the MPP to provide a significant amount of kinetic energy storage that can be used to provide inertia support. To fully leverage this capability, given the curtailment parameter $\eta_{\rm del} \in \mathbb{R}_{[0,1]}$, we use $\lambda_{\rm del} \in \mathbb{R}_{\geq \lambda_{\rm mpp}}$ to denote the (unique) solution of

$$C_p(\lambda_{\rm del}, 0) = \eta_{\rm del} C_p(\lambda_{\rm mpp}, 0). \quad (11)$$

If $v_{\rm w} \leq R\omega^{\max}/\lambda_{\rm del}$ holds for the maximum rotor speed $\omega^{\max} \in \mathbb{R}_{>0}$, then the desired level of curtailment can be achieved purely by speed based curtailment, i.e., $\omega_{\rm ref} = \frac{\lambda_{\rm del}}{R} v_{\rm w}$ and $\beta_{\rm del} = 0$. Otherwise, $\omega_{\rm ref} = \omega^{\max}$ and the curtailed pitch angle reference $\beta_{\rm del}$ is given by the solution of

$$C_p(\tfrac{R\omega^{\max}}{v_{\rm w}}, \beta_{\rm del}) = \eta_{\rm del} C_p(\lambda_{\rm mpp}, 0) \quad (12)$$

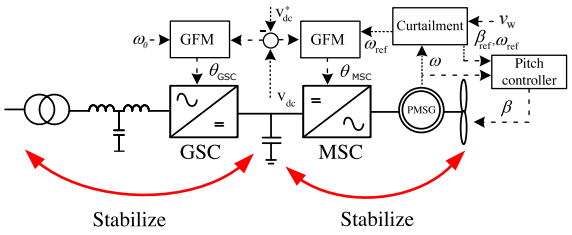

Fig. 12: PMSG wind turbine with dual-port GFM control for both GSC and MSC.

that satisfies $\lambda_{\text{del}} \geq \lambda_{\text{mpp}}$. Using the models presented in Sec. II, an equivalent droop coefficient shown in Fig. 13 and inertia coefficient can be directly computed as a function of the curtailment $\eta_{\text{del}} \in \mathbb{R}_{[0,1]}$ [20].

Finally, the simulated response of an aggregate model of ten 5 MW PMSG wind turbines to a load step is shown in Fig. 14. It can be seen that, depending on the operating point, dual-port GFM control either results in MPPT or releases the excess kinetic energy stored in the wind turbine rotor to provide an inertia response and primary frequency control. This illustrates that (9) enables a wind turbine to support MPPT control and ancillary services without switching controls.

C. End-to-end stability analysis for dual-port GFM control

A particularly appealing feature of the dual-port GFM control (9) and its power-balancing variant proposed in [24] is that it is amenable to an end-to-end stability analysis that encompasses reduced-order models of renewable generation (curtailed and at MPP), ac and dc transmission, and legacy generation [21], [24]. Specifically, the overall power system

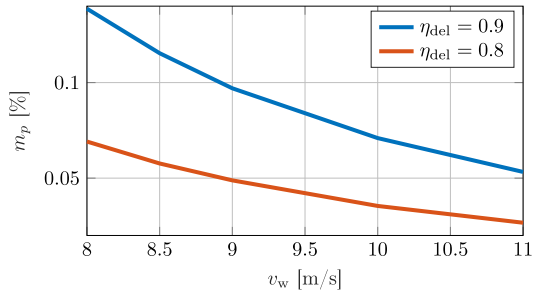

Fig. 13: Equivalent frequency droop coefficient for a PMSG wind turbine with curtailment according to (11) and (8).

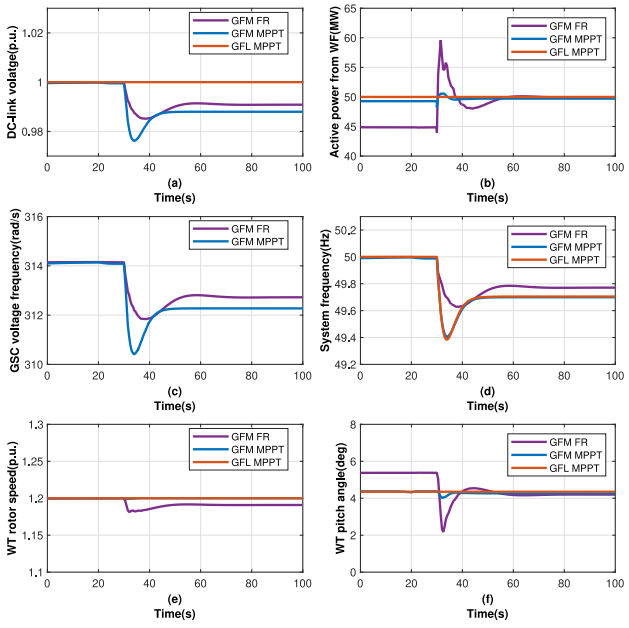

Fig. 14: Response of a wind turbine to a load step using ac-GFL MPPT control (GFL MPPT) and dual-port GFM control with (GFM FR) and without (GFM MPPT) curtailment.

can be modeled as graph whose nodes and edges correspond to linearized device models presented in Sec. II. Then, under mild conditions on the network topology, insightful conditions for synchronization and stability of frequency and dc voltage can be developed. Notably, frequency synchronization can be guaranteed for a wide range of standard networks including those shown in Fig. 4. In addition, if sufficiently many renewable generation with curtailment or legacy generation with primary frequency control are present, then frequency and dc voltage stability can be guaranteed. Under mild assumptions, the results can be extended to account for $N-1$ security criteria to ensure stability under the loss of any generating unit, ac line, or dc line.

VI. Conclusions and Outlook

In this tutorial we provided an overview of modeling and control of grid-connected power electronics and renewable generation. After an introduction to modeling of prevalent power generation and power conversion technologies, we discussed applications of GFL and GFM control to renewable generation. We highlighted the need for further research on interoperability of GFM control, GFL control, and legacy devices. Finally, this tutorial briefly discussed recent work on dual-port GFM control that supports the entire range of functions of GFL control (e.g., MPPT) and GFM control (e.g., primary frequency control) in a single universal controller and enables an end-to-end stability analysis using reduced-order models. GFM control under constraints (e.g., VSC current limits, wind turbine speed limits) is seen as an interesting area for future work.

References

[1] W. Winter, K. Elkington, G. Bareux, and J. Kostevc, "Pushing the limits: Europe's new grid: Innovative tools to combat transmission bottlenecks and reduced inertia," *IEEE Power Energy Mag.*, vol. 13, no. 1, pp. 60–74, 2015.

[2] B. Kroposki *et al.*, "Achieving a 100% renewable grid: Operating electric power systems with extremely high levels of variable renewable energy," *IEEE Power Energy Mag.*, vol. 15, no. 2, pp. 61–73, 2017.

[3] J. Matevosyan *et al.*, "Grid-forming inverters: Are they the key for high renewable penetration?" *IEEE Power Energy Mag.*, vol. 17, no. 6, pp. 89–98, 2019.

[4] F. Dörfler and D. Groß, "Control of low-inertia power systems," *Annual Review of Control, Robotics, and Autonomous Systems*, vol. 6, no. 1, pp. 415–445, 2023.

[5] D. Callaway and I. Hiskens, "Achieving controllability of electric loads," *Proc. IEEE*, vol. 99, no. 1, pp. 184–199, 2011.

[6] A. L. F. Acevedo *et al.*, "Design and valuation of high-capacity HVDC macrogrid transmission for the continental US," *IEEE Trans. Power Syst.*, vol. 36, no. 4, pp. 2750–2760, 2021.

[7] J. Rocabert, A. Luna, F. Blaabjerg, and P. Rodríguez, "Control of power converters in ac microgrids," *IEEE Trans. Power Electron.*, vol. 27, no. 11, pp. 4734–4749, 2012.

[8] U. Markovic, O. Stanojev, P. Aristidou, E. Vrettos, D. Callaway, and G. Hug, "Understanding small-signal stability of low-inertia systems," *IEEE Trans. Power Syst.*, vol. 36, no. 5, pp. 3997–4017, 2021.

[9] F. Dörfler and F. Bullo, "Synchronization and transient stability in power networks and nonuniform kuramoto oscillators," *SIAM Journal on Control and Optimization*, vol. 50, no. 3, pp. 1616–1642, 2012.

[10] J. Schiffer, R. Ortega, A. Astolfi, J. Raisch, and T. Sezi, "Conditions for stability of droop-controlled inverter-based microgrids," *Automatica*, vol. 50, no. 10, pp. 2457–2469, 2014.

[11] L. Pao and K. Johnson, "Control of wind turbines," *IEEE Control Syst. Mag.*, vol. 31, no. 2, pp. 44–62, 2011.

[12] J. Aho, P. Fleming, and L. Y. Pao, "Active power control of wind turbines for ancillary services: A comparison of pitch and torque control methodologies," in *American Control Conference*, 2016, pp. 1407–1412.

[13] A. F. Hoke, M. Shirazi, S. Chakraborty, E. Muljadi, and D. Maksimović, "Rapid active power control of photovoltaic systems for grid frequency support," *IEEE Trans. Emerg. Sel. Topics Power Electron.*, vol. 5, no. 3, pp. 1154–1163, 2017.

[14] A. Tayyebi, D. Groß, A. Anta, F. Kupzog, and F. Dörfler, "Frequency stability of synchronous machines and grid-forming power converters," *IEEE Trans. Emerg. Sel. Topics Power Electron.*, vol. 8, no. 2, pp. 1004–1018, 2020.

[15] X. Lyu and D. Groß, "Grid forming fast frequency response for pmsg-based wind turbines," *IEEE Trans. Sustain. Energy*, 2023.

[16] A. Crivellaro, A. Tayyebi, C. Gavriluta, D. Groß, A. Anta, F. Kupzog, and F. Dörfler, "Beyond low-inertia systems: Massive integration of grid-forming power converters in transmission grids," in *IEEE PES General Meeting*, 2020.

[17] J. A. Soler, D. Groß, E. P. Araujo, and O. G. Bellmunt, "Interconnecting power converter control role assignment in grids with multiple ac and dc subgrids," *IEEE Trans. Power Del.*, vol. 38, no. 3, pp. 2058–2071, 2023.

[18] R. H. Lasseter, Z. Chen, and D. Pattabiraman, "Grid-forming inverters: A critical asset for the power grid," *IEEE Trans. Emerg. Sel. Topics Power Electron.*, vol. 8, no. 2, pp. 925–935, 2020.

[19] S. Wang and K. Tomsovic, "Fast frequency support from wind turbine generators with auxiliary dynamic demand control," *IEEE Trans. Power Syst.*, vol. 34, no. 5, pp. 3340–3348, 2019.

[20] X. Lyu, I. Subotić, and D. Groß, "Unified grid-forming control of pmsg wind turbines for fast frequency response and MPPT," in *IREP Bulk Power System Dynamics and Control Symposium*, 2022.

[21] I. Subotić, , and D. Groß, "Universal dual-port grid-forming control: bridging the gap between grid-forming and grid-following control," 2023, arXiv:2304.04939.

[22] D. Groß, E. Sánchez-Sánchez, E. Prieto-Araujo, and O. Gomis-Bellmunt, "Dual-port grid-forming control of MMCs and its applications to grids of grids," *IEEE Trans. Power Del.*, vol. 37, no. 6, pp. 4721–4735, 2022.

[23] I. Subotić and D. Groß, "Energy-balancing dual-port grid-forming control for VSC-HVDC systems," in *IFAC World Congress*, 2023.

[24] I. Subotić; and D. Groß, "Power-balancing dual-port grid-forming power converter control for renewable integration and hybrid AC/DC power systems," *IEEE Trans. Control Netw. Syst.*, 2022.

[25] P. Kundur, *Power System Stability and Control*. McGraw-Hill, 1994.

[26] T. Knudsen and T. Bak, "Simple model for describing and estimating wind turbine dynamic inflow," in *American Control Conference*, 2013, pp. 640–646.

[27] M. G. Villalva, J. R. Gazoli, and E. R. Filho, "Comprehensive approach to modeling and simulation of photovoltaic arrays," *IEEE Trans. Power Electron.*, vol. 24, no. 5, pp. 1198–1208, 2009.

[28] P. Monshizadeh, C. De Persis, N. Monshizadeh, and A. J. van der Schaft, "Nonlinear analysis of an improved swing equation," in *IEEE Conference on Decision and Control*, 2016, pp. 4116–4121.

[29] O. Ajala, A. Domínguez-García, P. Sauer, and D. Liberzon, "A library of second-order models for synchronous machines," *IEEE Trans. Power Syst.*, vol. 35, no. 6, pp. 4803–4814, 2020.

[30] A. Yazdani and R. Iravani, *Voltage-Sourced Converters in Power Systems: Modeling, Control, and Applications*. Wiley, 2010.

[31] H. W. Dommel, "Digital computer solution of electromagnetic transients in single-and multiphase networks," *IEEE Trans. Power App. Syst.*, vol. PAS-88, no. 4, pp. 388–399, 1969.

[32] A. Morched, B. Gustavsen, and M. Tartibi, "A universal model for accurate calculation of electromagnetic transients on overhead lines and underground cables," *IEEE Trans. Power Del.*, vol. 14, no. 3, pp. 1032–1038, 1999.

[33] J. Beerten, S. D'Arco, and J. Suul, "Cable model order reduction for HVDC systems interoperability analysis," in *IET International Conference on AC and DC Power Transmission*, 2015.

[34] F. Dörfler, J. W. Simpson-Porco, and F. Bullo, "Electrical networks and algebraic graph theory: Models, properties, and applications," *Proc. IEEE*, vol. 106, no. 5, pp. 977–1005, 2018.

[35] S. Fiaz, D. Zonetti, R. Ortega, J. Scherpen, and A. van der Schaft, "A port-hamiltonian approach to power network modeling and analysis," *European Journal of Control*, vol. 19, no. 6, pp. 477–485, 2013, lagrangian and Hamiltonian Methods for Modelling and Control.

[36] P. W. Sauer and M. A. Pai, *Power System Dynamics and Stability*. Prentice Hall, 1998.

[37] O. Gomis-Bellmunt, E. Sánchez-Sánchez, J. Arévalo-Soler, and E. Prieto-Araujo, "Principles of operation of grids of DC and AC subgrids interconnected by power converters," *IEEE Trans. Power Del.*, vol. 36, no. 2, pp. 1107–1117, 2021.

[38] P. Vorobev, P.-H. Huang, M. Al Hosani, J. L. Kirtley, and K. Turitsyn, "High-fidelity model order reduction for microgrids stability assessment," *IEEE Trans. Power Syst.*, vol. 33, no. 1, pp. 874–887, 2018.

[39] D. Groß, M. Colombino, B. Jean-Sébastien, and F. Dörfler, "The effect of transmission-line dynamics on grid-forming dispatchable virtual oscillator control," *IEEE Trans. Control Netw. Syst.*, vol. 6, no. 3, pp. 1148–1160, 2019.

[40] I. Subotić, D. Groß, M. Colombino, and F. Dörfler, "A Lyapunov framework for nested dynamical systems on multiple time scales with application to converter-based power systems," *IEEE Trans. Autom. Control*, vol. 66, no. 12, pp. 5909–5924, 2021.

[41] D. Groß, "Compensating network dynamics in grid-forming control," in *Allerton Conference on Communication, Control, and Computation*, 2022.

[42] A. Bernstein, C. Wang, E. Dall'Anese, J.-Y. Le Boudec, and C. Zhao, "Load flow in multiphase distribution networks: Existence, uniqueness, non-singularity and linear models," *IEEE Trans. Power Syst.*, vol. 33, no. 6, pp. 5832–5843, 2018.

[43] K. Girigoudar and L. A. Roald, "Linearized three-phase optimal power flow models for distribution grids with voltage unbalance," in *IEEE Conference on Decision and Control*, 2021, pp. 4214–4221.

[44] S. S. Nudehi and D. Groß, "Grid-forming control of three-phase and single-phase converters across unbalanced transmission and distribution systems," *IEEE Trans. Power Syst.*, 2022.

[45] D. Sehloff and L. A. Roald, "Low frequency AC transmission upgrades with optimal frequency selection," *IEEE Trans. Power Syst.*, vol. 37, no. 2, pp. 1437–1448, 2022.

[46] M.-S. Debry, G. Denis, and T. Prevost, "Characterization of the grid-forming function of a power source based on its external frequency smoothing capability," in *IEEE PowerTech*, 2019.

[47] D. Ramasubramanian *et al.*, "Performance specifications for grid-forming technologies," in *IEEE Power & Energy Society General Meeting*, 2023.

[48] H.-P. Beck and R. Hesse, "Virtual synchronous machine," in *International Conference on Electrical Power Quality and Utilisation*, 2007.

[49] S. D'Arco, J. A. Suul, and O. B. Fosso, "A virtual synchronous machine implementation for distributed control of power converters in smartgrids," *Electr. Pow. Sys. Res.*, vol. 122, pp. 180–197, 2015.

[50] D. Dong, B. Wen, D. Boroyevich, P. Mattavelli, and Y. Xue, "Analysis of phase-locked loop low-frequency stability in three-phase grid-connected power converters considering impedance interactions," *IEEE Trans. Ind. Electron.*, vol. 62, no. 1, pp. 310–321, 2015.

[51] Y. Lin, G.-S. Seo, S. Vijayshankar, B. Johnson, and S. Dhople, "Impact of increased inverter-based resources on power system small-signal stability," in *IEEE Power & Energy Society General Meeting*, 2021.

[52] Y. Li, Y. Gu, and T. C. Green, "Revisiting grid-forming and grid-following inverters: A duality theory," *IEEE Trans. Power Syst.*, vol. 37, no. 6, pp. 4541–4554, 2022.

[53] S. D'Arco, J. A. Suul, and O. B. Fosso, "A virtual synchronous machine implementation for distributed control of power converters in smartgrids," *Electr. Pow. Sys. Res.*, vol. 122, pp. 180–197, 2015.

[54] M. Chandorkar, D. Divan, and R. Adapa, "Control of parallel connected inverters in standalone ac supply systems," *IEEE Trans. Ind. Appl.*, vol. 29, no. 1, pp. 136–143, 1993.

[55] I. Cvetkovic, D. Boroyevich, R. Burgos, C. Li, and P. Mattavelli, "Modeling and control of grid-connected voltage-source converters emulating isotropic and anisotropic synchronous machines," in *Workshop on Control and Modeling for Power Electronics*, 2015.

[56] S. Curi, D. Groß, and F. Dörfler, "Control of low-inertia power grids: A model reduction approach," in *IEEE Conference on Decision and Control*, 2017, pp. 5708–5713.

[57] I. Subotiċ, D. Groß, M. Colombino, and F. Dörfler, "A Lyapunov framework for nested dynamical systems on multiple time scales with application to converter-based power systems," *IEEE Trans. Autom. Control*, vol. 66, no. 12, pp. 5909–5924, 2021.

[58] S. Bala and G. Venkataramanan, "On the choice of voltage regulators for droop-controlled voltage source converters in microgrids to ensure stability," in *IEEE Energy Conversion Congress and Exposition*, 2010, pp. 3448–3455.

[59] T. Qoria, F. Gruson, F. Colas, X. Guillaud, M. Debry, and T. Prevost, "Tuning of cascaded controllers for robust grid-forming voltage source converter," in *Power Systems Computation Conference*, 2018.

[60] B. Johnson, S. Salapaka, B. Lundstrom, and M. Salapaka, "Optimal structures for voltage controllers in inverters," in *IEEE International Symposium on Mathematical Theory of Networks and Systems*, 2016.